ELSEVIER

Catalysis Today 25 (1995) 365–370

CATALYSIS TODAY

Equilibrium-shift in alkane dehydrogenation using a high-temperature catalytic membrane reactor

E. Gobina *, K. Hou, R. Hughes

Department of Chemical Engineering, University of Salford, Salford, M5 4WT, UK

Abstract

This study involves the application of a tubular fixed-bed catalytic membrane reactor to effect equilibrium-shift during the catalytic dehydrogenation of ethane to ethylene and hydrogen. The specific characteristic behaviour of the reactor to shift the equilibrium was analysed using a two-dimensional mathematical model which was solved using the orthogonal collocation method. An important extrinsic variable, the time factor (W/F_{A_0}) was manipulated to yield results which were then used to explain reactor performance. Experimental results showed that under optimal conditions an eight-fold shift in the equilibrium conversion could be attained. Generally, good agreement was obtained between model and experimental predictions for reactor operation using pure nitrogen as sweep gas. When air was employed as sweep, the agreement was not as expected; possibly due to oxidation of the Pd surface.

1. Introduction and background

Porous ceramic membranes (ca. 40 Å pore size) have been widely applied in high-temperature gas-phase equilibrium limited dehydrogenation reactions to enhance conversion [1,2]. Dense membranes having exclusive hydrogen permeability have also received wide attention [3,4]. With porous membranes (ceramic or glass) there is always some 'slip' of reactants through the porous matrix which therefore limits the maximum achievable conversion. Commercially available dense membranes supplied as foils (ca. 25 μm) or as thick walled tubes (ca. 63 μm) are too thick to give sufficient hydrogen fluxes and because of the amount of material involved represent a high cost of precious metal. New developments in ceramic and thin film technology have made it possible to combine the high H_2 flux of thin but continuous metallic films with the mechanical strength of porous substrates. Such composite structures offer clear advantages over either thick metallic foils (or tubes), or porous membranes. These composite structures therefore possess the potential of forming the basis of the next generation of catalyst–membrane systems. Such membrane systems could well become important in the future for enhancing the conversion of industrially important equilibrium limited dehydrogenation reactions through high single-pass conversions at reduced operating temperatures.

2. Present investigation

2.1. Experimental

The key elements of the membrane used in the present study consisted of a continuous 6-μm

* Corresponding author.

SSDI 0920-5861(95)00115-8

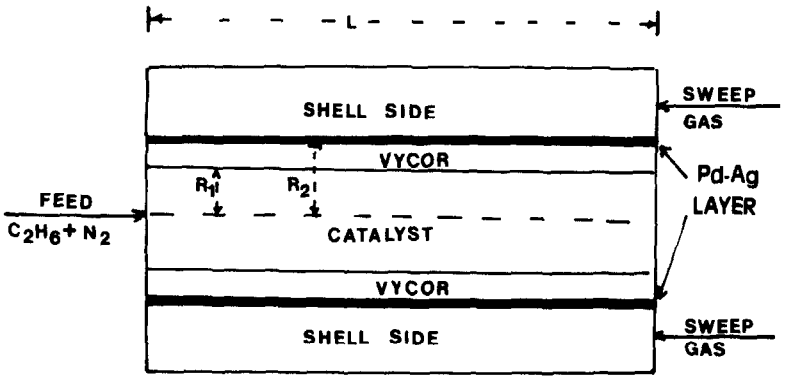

Fig. 1. Schematic diagram of the membrane reactor operation.

thick film of Pd–23% Ag alloy deposited on the outside surface of a porous Vycor glass tube (10 mm O.D. and 1.1 mm wall thickness) which was housed within a stainless steel shell using compressible moulded graphite rings. The film was deposited by magnetron sputtering and was characterised by a variety of techniques including scanning electron microscopy (SEM), relative light transmission, electrical resistivity and electron probe micro-analysis (EPMA). These tests showed that the films were coherent and pinhole free with excellent adhesion to the Vycor substrate. The absence of pinholes was confirmed by pressure tests using nitrogen. Furthermore, the EPMA analysis demonstrated that the film composition was identical with the original target material at 23% Ag content. Transport of hydrogen through the membrane obtained by separate experimentation [5] gave agreement with Sieverts Law [6]. In the present experiments, a mixture of 50% ethane in nitrogen was used and fed to the inside of the tubular membrane, which was packed with a 0.5% Pd on γ-alumina catalyst in the form of 3 mm equant cylindrical pellets. The outer (shell) side of the membrane could be swept with either a pure nitrogen or air purge. Throughout all the experiments the bed temperature was maintained at 660 K; the variation along the length of the reactor was observed to be within ± 2°C throughout all experiments. At the relatively low-reaction temperature of 660 K employed in this work, no catalyst deactivation was detected.

2.2. Mathematical model

The basic assumptions and details of the development of the two-dimensional mathematical model have been presented elsewhere [7], but are listed briefly as follows:

(1) Isothermal conditions prevail.
(2) Temperature and pressure gradients in the catalyst pellet may be neglected.
(3) Operation is steady state.
(4) The pressure in the catalyst bed and Vycor glass is constant because of the low conversion of ethane.
(5) Any change in pressure in the sweep gas due to hydrogen permeation may be neglected because of the small extent of permeation compared to sweep flow rate.
(6) Axial dispersion is neglected but radial dispersion in both the catalytic bed and Vycor glass are accounted for.
(7) Radial changes of concentration are included in the model.
(8) Changes in flow rate along the reactor length are negligible due to the low conversion obtained.

Fig. 1 shows the main features schematically. Balances for C_2H_6 (1), C_2H_4 (2), H_2 (3) and N_2 (4) may be written in dimensionless form as follows:

In the catalytic bed, $0 < r_1 < 1$, where r_1 is the dimensionless radius

$$\frac{\partial y_i}{\partial \xi} = \frac{\alpha}{P_{ei}} \frac{1}{r_1} \frac{\partial}{\partial r_1} \left[r_1 \frac{\partial y_1}{\partial r_1} \right] + r_A \qquad (1)$$

where $i=1, 2, 3$ and 4 as indicated above and α and P_{ei} represent a constant and a Peclet number respectively and the other symbols are given in the Nomenclature.

In the porous Vycor glass substrate, $r_2=(r-R_1)/(R_2-R_1)$

$$\frac{\Delta R}{r_2\Delta R+R_1}\frac{\partial}{\partial r_2}\left(\frac{r_2\Delta R+R_1}{\Delta R}\frac{\partial x_i}{\partial r_2}\right)=0 \qquad (2)$$

For the membrane and shell side, the mole fraction of hydrogen in the sweep gas, y_s, is given by ($\gamma=0$, pure N_2 sweep; $\gamma=1$, air as sweep) and $m=1$ (countercurrent) and $m=2$ (cocurrent).

$$\frac{dy_s}{d\xi}=(-1)^m d_1[(y_3^{1/2}-(P_r)^{1/2}y_3^{1/2}] -(-1)^m\gamma r_{H_2} \qquad (3)$$

where the symbols are defined in the nomenclature; r_{H_2} is the dimensionless reaction rate between the permeated hydrogen and oxygen in the air sweep gas.

The boundary conditions for Eqs. (1) to (3) are:

$$r_1=0,\quad \frac{\partial y_i}{\partial r}=0,\quad i=1,2,3,4 \qquad (4)$$

$$r_2=0,\quad r_1=0,\quad y=x_i$$

$$\left.\frac{\partial y_i}{\partial r_1}\right|_{r_1=1}=d_2\left.\frac{\partial x_i}{\partial r_2}\right|_{r_2=0}\Bigg\}i=1,2,3,4 \qquad (5)$$

$$r_2=1,\quad \frac{\partial x_i}{\partial r_2}r_{2=1}=0,\quad i=1,2,4 \qquad (6)$$

$$\left.\frac{\partial x_3}{\partial R_2}\right|_{r_2=1}=-d_3[y_3^{1/2}-y_s^{1/2}(P_r)^{1/2}] \qquad (7)$$

$$\xi=0\left\{y_1=1,\ y_2=y_3=0,\ y_4=\frac{C_{40}}{C_{10}},\right.$$

$y_s=0$ for cocurrent flow (8)

$\xi=1\quad y_s=0$ (for countercurrent flow) (9)

Eq. (3) together with boundary conditions (5) to (7) gives: for $i=1, 2$ and 4,

$$\text{At any } \xi\left\{x_i=y_i|_{r_1=1},\quad \frac{\partial x_i}{\partial r_2}=0\right. \qquad (10)$$

For $i=3$

$$x_3=\frac{d_3R_2}{\Delta R}[y_3^{1/2}-(P_r^{1/2})y_s^{1/2}]\ \ln\left[\frac{R_1}{r_2\Delta R+R_1}\right] +y_3|_{r_1=1} \qquad (11)$$

The system of Eqs. (1) to (3) and boundary conditions (4) to (11) form a set of partial differential equations of the boundary value type (countercurrent flow). The first and second order derivatives were discretised using four collocation points to yield a set of ordinary differential equations which were solved using the fourth order Runge–Kutta routine using an initial guessed value for at $\xi=0$.

For the coupling reaction, using air as sweep gas the kinetics of Leder and Butt [9] were used for the reaction of the permeated hydrogen with oxygen.

2.3. Reaction kinetics

The kinetics of the reaction were determined by operating in a fixed-bed reactor mode i.e. the shell-side inlet and exit were closed. The reaction temperature, contact time and ethane concentration were varied and the effluent concentrations of the reacting species analysed on-line by gas-chromatography. The reaction order with respect to ethane concentration was found to be first order, and since the concentrations of hydrogen and ethylene were very small, first order dependencies were assumed for these species. An Arrhenius plot of the reaction rate enabled the activation energy to be determined. The reaction rate was then used to predict conversion levels during membrane reactor operation. An optimization search was used to obtain the best pre-exponential factor value by minimisation of the sum of errors of the residual squares $\Sigma\Delta^2$, between experimentally determined conversions and predicted conversions as given by Eq. (12):

$$\sum_{i-1}^{n} \Delta i^2 = \sum_{i-1}^{n} \left[\frac{X_{C_2H_6,i}(\text{exp}) - X_{C_2H_6,i}(\text{pred})}{X_{C_2H_6,i}(\text{exp})}\right]^2 \quad (12)$$

The kinetic expression obtained following this procedure was then given by:

$$r_A = 4.39 \exp\left[\frac{-75580}{RT}\right][P_{C_2H_6} - P_{C_2H_4}P_{H_2}/K_e] \quad (13)$$

which may be written in dimensionless form as

$$\bar{r}_A = \alpha_i \rho_B r_A \quad (14)$$

The activation energy value obtained in this work was in good agreement with the value quoted with literature [8] for the dehydrogenation of ethane over a Pt/Al_2O_3 catalyst. Predicted ethane conversions were within 15% of the measured values in the region of interest in this study.

3. Results and discussion

3.1. Membrane permeability characteristics

The flux of hydrogen through the composite membrane was found to obey the half-power pressure law indicating that flow through the metal was rate limiting. This flux was also found to increase with an increase in temperature at any fixed pressure differential. From a plot of ln Q_o, the permeability constant versus the inverse temperature the activation energy and pre-exponential factor for H_2 permeation were obtained. The rate of hydrogen transport across the composite membrane (Q_H; cm^3/s) was then given by Eq. (15).

$$Q_H = 7.174 \times 10^{-5} \exp(-6.380/RT)(P_1^{1/2} - P_2^{1/2})(A/d_t) \quad (15)$$

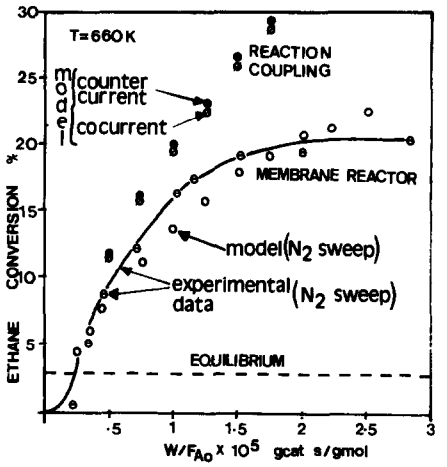

Fig. 2. Comparison of experimental and modelling results for ethane hydrogenation.

3.2. Characteristics of membrane reactor performance

Membrane reactor behaviour was analysed by obtaining quantitative information during the variation of the time factor (W/F_{Ao}) as shown in Fig. 2. At high gas velocities, the residence time of ethane in the reactor is low resulting in very low conversions (below the equilibrium value). Under these conditions the partial pressure of hydrogen in the tube-side is too small to effect any shift in the equilibrium. As the contact time increases, the hydrogen partial pressure difference increases and hydrogen permeation begins to control the ethane conversion (ca. $0.25 \leq W/F_{Ao} \leq 1) \times 10^5$). The effectiveness of the membrane reactor to shift the conversion is clearly evident with the steep rise in conversion between $1.0 < W/F_{Ao} \leq 2.0 \times 10^5$. In this region, our calculations indicate that the permeation rate was roughly 6–7 times the production rate; in other words, this is the region of high performance. Higher contact times did not result in enhanced ethane conversion ($W/F_{Ao} \geq 2.0 \times 10^5$). We speculate that possible readsorption of hydrogen and ethylene in this region prevents any net change in the hydrogen driving force thus resulting in a new equilibrium level. It is well known that these species are strongly adsorbed on Pd/Al_2O_3 catalysts. Furthermore, the BET surface

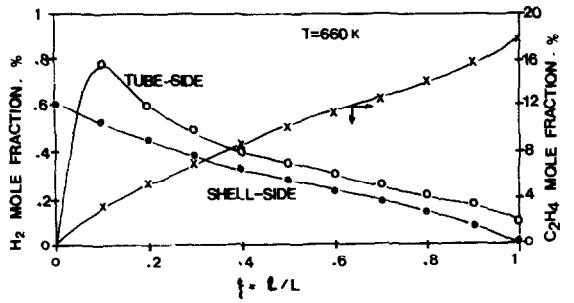

Fig. 3. Simulated axial species concentration profiles.

area of the catalyst was large (ca. 280 m^2/g), which would suggest a strong possibility of readsorption. Fig. 3 shows simulated profiles of the hydrogen mole fraction in the shell and tube sides of the membrane reactor for countercurrent operation, as well as the ethylene production rate. It can be seen that the latter increases monotonically with bed length whereas the hydrogen in the tube side shows a peak concentration near the reactor inlet due to the dehydrogenation reaction. On the shell side however, there is a steady increase in hydrogen concentration because of the countercurrent flow of purge gas. When air was used as sweep gas (oxidative extraction) model predictions did not give good agreement with experimental data. This was attributed to the oxidation of the Pd surface which then prevents hydrogen recombination.

Although the model allowed for the possibility of radial concentration variation, the radial profiles obtained showed virtually no difference in concentration for all four species concerned. Therefore a plug flow reactor model could be used for future work using a reactor of similar dimensions.

4. Conclusions

A comprehensive mathematical model has been developed and used to investigate the characteristic behaviour of a fixed-bed tubular membrane reactor for light alkane dehydrogenation. An eight-fold enhancement of the equilibrium conversion was achievable at high reactor performance. The model has been validated with experimental data and would therefore facilitate the procurement of preliminary design parameters for interpreting and explaining observed reactor behaviour.

5. Nomenclature

A	= Membrane area
C	= Concentration
d_t	= Pd–Ag thickness
d_1	$= 2\pi R_2 L Q_{H2} P_t^{1/2} / (Q_s \cdot \delta)$
d_2	$= \epsilon_2 / \epsilon_1 \cdot R_1 / \Delta R$
d_3	$= \Delta R Q_{H_2} P_t^{1/2} / (22400\, C_{10}\, \epsilon_2\, D_2 \cdot \delta)$
D_i	= diffusivity of component i in mixture
L	= length of catalyst bed
P	= pressure
P_r	$= P_s / P_t$ = pressure ratio (shell side to tube side)
Q_{H_2}	= permeation flux of H_2
Q_s	= sweep gas flow rate
r_A	$= \alpha \rho_B r_A$
r_{H_2}	$= 44800 \pi R_2 L r_{H_2} / Q_s$
r_1	$= r / R_1$ = dimensionless radius in bed
r_2	$= (r - R_1) / (R_2 - R_1)$ dimensionless radius in Vycor glass
R_1	= inner radius of Vycor glass
R_2	= outer radius of Vycor glass
ΔR	= thickness of Vycor glass
U_o	= Superficial gas velocity
x	= dimensionless concentration in Vycor glass
y	= component concentration in reactor bed
α	$= \epsilon_1 L^2 / l^2$
α_i	$= v_i L / (U_o C_{10})$
δ	= thickness of membrane
ϵ_1	= porosity of catalyst bed
ϵ_2	= porosity of Vycor glass
v	= stoichiometric coefficient ($v_1 = -1$, $v_2 = v_3 = 1$, $v_4 = 0$)
ρ_B	= catalyst bed density
ξ	= dimensionless bed length

Subscripts

i	= component of mixture
0	= inlet value
s	= sweep side
t	= tube (reaction) side

Acknowledgements

Thanks are due to the EPSRC for the continued support for this research. We are also grateful to Johnson Matthey plc for the characterisation of the catalysts and EPMA on the Pd–Ag alloy membranes. Magnetron depositions were undertaken by Dr. D. Monaghan to whom we express our sincere gratitude.

References

[1] Y.L. Becker, A.G. Dixon, W.R. Moser and Y.H. Ma, J. Membrane Sci., 77 (1993) 233.
[2] Z.O. Ziaka, R.G. Minet and T.T. Tsotsis, J. Membrane Sci., 77 (1993) 221.
[3] N. Itoh, AIChE J., 33 (1987) 1576.
[4] A.W. Wang, B.D. Raich, B.K. Johnson and H.C. Foley, Prepr. Am. Chem. Soc., Div. Pet. Chem., 37 (3) (1992) 743.
[5] E. Gobina and R. Hughes, Dev. Chem. Eng. Min. Process., 2 (1994) 105.
[6] A. Sieverts and W. Kumbhaar, Ber. Deut. Chem. Gas., 43 (1910) 893.
[7] E. Gobina, K. Hou and R. Hughes, Chem. Eng. Sci. (1995).
[8] A.M. Champagnie, T.T. Tsotsis, R.G. Minet and I.A. Webster, Chem. Eng. Sci., 45 (1990) 2423.
[9] H. Leder and J.B. Butt, AIChE J., 12 (1966) 718.